Interacting straight-sided buckles: An enhanced attraction by substrate elasticity

C. Coupeau, Romain Boijoux, Y. Ni, G. Parry

Interacting straight-sided buckles: An enhanced attraction by substrate elasticity

C. Coupeau [a, c, *], R. Boijoux [a, b], Y. Ni [c], G. Parry [b]

[a] Institut Pprime, Department of Physics and Mechanics of Materials, UPR 3346 CNRS-ENSMA-Université de Poitiers, 86000 Poitiers, France

[b] SIMaP, UMR 5266 CNRS, Université de Grenoble-Alpes, Grenoble 38000, France

[c] CAS Key Laboratory of Mechanical Behavior and Design of Materials, University of Science and Technology of China, Hefei, Anhui 230026, PR China

A B S T R A C T

Interaction between two straight-sided buckles propagating in opposite directions has been investigated by atomic force microscopy. Below a critical separation distance, it is observed that the two buckles are attracted towards each other once their fronts have crossed. A mechanical analysis using finite element simulations has shown that the buckle interaction is strongly influenced by the substrate elasticity. The deviation of the two buckles from their initial straight propagation is discussed at the light of mode mixity mappings extracted from finite elements simulations along the crack path of the two interacting buckles. Finally, a phase diagram depending on both the separation distance and the film/substrate elastic mismatch is proposed, in good agreement with the experimental results.

1. Introduction

Thin films and coatings are widely used in a large variety of application domains, such as for instance thermal barriers under extreme environments (Faulhaber et al., 2006), multilayers for optical performance (Karlsson et al., 1981) or improvements of mechanical properties as wear resistance (Charitidis, 2010). Thin films mainly produced by physical vapor sputtering techniques often develop high internal stresses, sometimes about a few GPa in compression (see Abadias et al., 2018 for a review). They are then susceptible to undergo delamination and buckling resulting in various patterns such as circular blisters, telephone cords or straight-sided buckles (Yu et al., 2013; Gioia and Ortiz, 1998; Moon et al., 2002; Yu et al., 2014; Faou et al., 2017; Jagla, 2007; Cordill et al., 2007; Ni et al., 2017). Preventing the buckling process is consequently a key point in coating technology, since delamination generally results in the loss of specific functional properties that were initially conferred to the coated materials.

The buckling phenomenon of thin films and coatings has been extensively analyzed during the last decades, in particular in the framework of Föppl-von Karman (FvK) theory of thin plates (Hutchinson and Suo, 1991). Some key effects of the substrate elasticity on buckling have been characterized (Yu and Hutchinson, 2002; Parry et al., 2005; Boijoux et al., 2017). Studies have been also focused on the effect of environment, such as for instance buckling induced by moisture on inorganic layers (Abdallah et al., 2008) or by traction in the transverse direction for metal/polymer systems

(Toth et al., 2013). From a mechanical point of view, it is now well-established that the mode mixity at the crack front plays a key-role on the growth of the buckles (Hutchinson and Suo, 1991). In particular, it was shown by finite elements simulations (FEM) that the telephone cord wavelength significantly depends on the film/substrate adhesion (Faou et al., 2015) and how the buckles may then develop up to a branching pattern (Jagla, 2007; Ni and Soh, 2014; Faou et al., 2017). In addition, a sliding mechanism at the interface highlighted by molecular dynamics simulations (Ruffini et al., 2012) was observed to control the buckling transition between a straight-sided buckle to a telephone cord (Pan et al., 2013), leading to selected wavelengths. Surprisingly, the interaction between elementary buckling structures remains mainly unexplored to the best of the authors knowledge. Neighbouring buckles propagating along parallel directions are however often observed on various thin films. It is the purpose of this work to investigate how two straight-sided buckles (SSB) interact. Experimental results are first presented and then compared to finite elements simulations taking into account the mode mixity dependence of the interface toughness at the crack front that was recently found to be significantly influenced by the elastic contrast between the film and its substrate (Boijoux et al., 2017).

2. Experiments

2.1. Materials and procedure

Ni films, 100 and 200 nm thick, have been deposited by physical vapor sputtering technique (PVD) on polycarbonate (PC) substrates. The Young's modulus of Ni and PC is $E_f = 200$ GPa and $E_s = 2.5$ GPa, respectively. It corresponds to a high elastic contrast between the film and the substrate characterized by a Dundur's parameter $\alpha = 0.94$ (Hutchinson and Suo, 1991). The internal stresses in the film, σ_0, induced by the PVD process (Abadias et al., 2018) have been estimated by curvature measurement using the Stoney method to be around a few hundreds of MPa in compression. The coated substrates were deformed using a home-made device allowing following *in situ* by atomic force microcopy (AFM), in air at room temperature, the surface evolution for increasing applied strains (Coupeau et al., 1998). Assuming a well-bonded film, the external stress σ_{yy} induced in the film is determined from the applied stress σ_a on the substrate by the following relation:

$$\sigma_{yy} = \frac{E_f}{E_s}\frac{1-\nu_f\nu_s}{1-\nu_f^2}\sigma_a, \tag{1}$$

with ν_f and ν_s, the Poisson's ratio of film and substrate, respectively.

The uniaxial compression of the substrates was performed in the following along the y axis, in order to induce straight-sided buckles (SSBs) lying perpendicularly (*i.e.* along the x direction), as usually observed in previous studies (Audoly et al., 2002; Parry et al., 2006).

2.2. Experimental results

The AFM observations of two SSBs propagating in parallel but opposite directions for the $h = 200$ nm thick Ni film are reported in Fig. 1, for two values of the σ_{yy} stress components. It is worth noting that similar evolutions have been also observed for the 100 nm thick Ni film but are not presented here for convenience.

When far away from each other, the SSB separation distance was determined to be $d = 12$ µm. Their widths are approximately equal to $2b \approx 10$ µm, which corresponds to a normalized distance $\bar{d} = d/2b \approx 1.2$. A surface feature has been used as a reference to position each AFM image (see the white ring). Both SSBs propagate following a straight path approximately lying along the x direction. As expected due to the high α value, each buckle equilibrium profile (called mexican hat in the literature) exhibits a depression on both edges close to the crack fronts (Parry et al., 2005). The AFM contrast has been enhanced in the insert (see black areas in Fig. 1a) to highlight these depressions measuring only a few nanometers depth.

As the buckle fronts are crossing (*i.e.* when the two fronts have reached approximately the same x value), the interaction is evidenced by their propagation trajectory from the x axis. The buckles seem to be attracted towards each other, leading to a kind of 'wrapping' of the two SBBs. Then, the two SSBs slightly continue to propagate for increasing σ_{yy} values, before reaching a point of arrest (Fig. 1b). No further evolution of the buckles has been observed beyond this state, even with a strong increase of the applied stress.

The interaction described previously usually occurs when two SSBs propagate towards each other. It is however interesting to note that a similar behavior is also frequently observed in the case where a SSB propagates towards an existing SSB that is slightly misoriented with respect to the first one (see for instance the grey arrows in Fig. 2).

3. FEM modeling

3.1. Configuration and assumptions

The mechanical model of our system of interest is composed of different regions (Fig. 3). The film is modeled by a geometrically non-linear plate, the substrate by a homogeneous three-dimensional solid. Both materials are assumed to be linear elastic isotropic. A thickness ratio of $h/H = 100$ is taken, with h (resp. H) the film (resp. the substrate) thickness. The dimensions of the cell along the x and y directions are respectively $2L_x$ and $2L_y$, with $L_x > L_y >> b_0$. The film is assumed

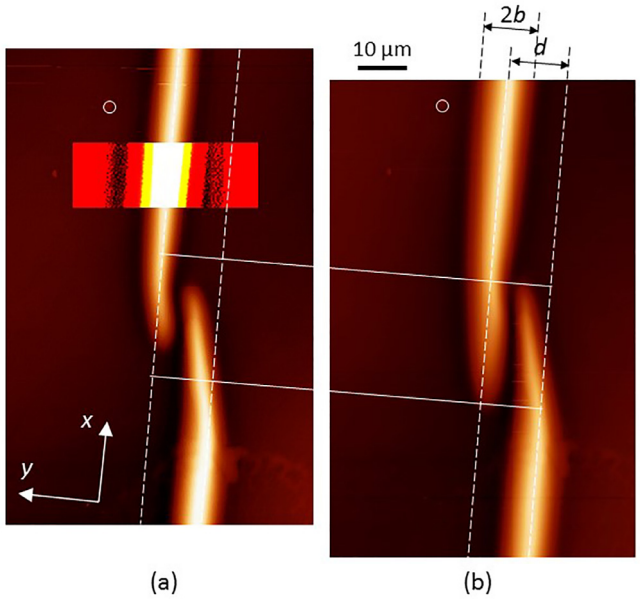

Fig. 1. Evolution of two SSBs propagating in opposite directions for two increasing σ_{yy} stress. Topographical AFM investigations at room temperature on a Ni 200 nm thick film on a PC substrate, for (a) $\sigma_{yy} = -105$ MPa (b) $\sigma_{yy} = -970$ MPa. The white circle is a surface marker used to position each image from the other. The initial separation distance between the two SBBs is labelled d and their width $2b$. The colour contrast has been enhanced in insert in (a) to highlight the nanometer-scale depression (black contrast) on both sides of the SSB.

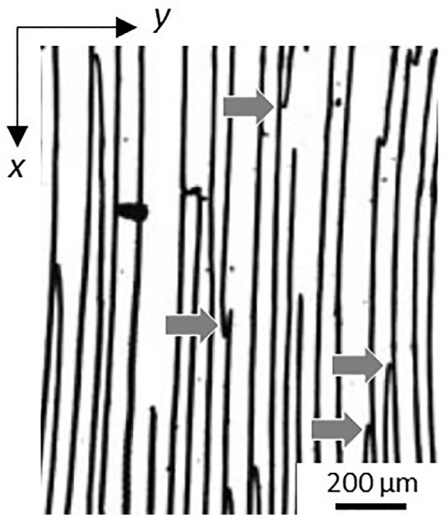

Fig. 2. Optical micrograph of a Ni 240 nm thick film deposited on a PC substrate strained at room temperature. The compression was carried out along the y axis.

to be initially bonded to its substrate except for two delaminated areas of width $2b_0$ separated from a distance d along the y direction. $2b_0$ is chosen just above the minimum width necessary for buckling to occur at the given applied stress (Hutchinson and Suo, 1991; Parry et al., 2006). Note that the choice of $2b_0$ does not impact the final width $2b$ of the SSB; it is just set to initiate the buckling/delamination process. The z direction is normal to the initial film/substrate interface plane. As far as the boundary conditions are concerned, all the sides of the simulation cell are left free, except for the faces normal to the y direction, at $y = \pm L_y$, where the compression occurs. On those two faces, the following displacements are prescribed: $u_x = u_z = 0$ and $u_y = \pm\tilde{U}$, with $\tilde{U}$ the value of the imposed displacement resulting from the substrate compression.

To simulate the interface debonding process, a mixed-mode cohesive zone (CZ) model is used, located all along the film/substrate interface. Cohesive zone models have been widely used in fracture mechanics over the past two decades (Tvergaard and Hutchinson, 1992; Xu and Needleman, 1993). They describe the constitutive behavior of the interface using a traction/separation law. Due to the interaction between the two separating faces, the interface traction vector $\vec{T}$ depends

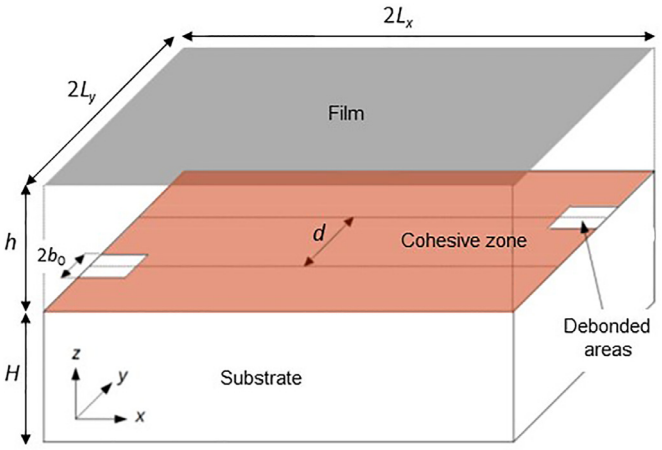

Fig. 3. FEM configuration of the film/substrate system. Two debonded areas of width $2b_0$ and separated from a distance d have been inserted at the film/substrate interface on both sides. h and H are the thickness of the film and of the substrate, respectively. $2L_x$ and $2L_y$ are the length of the simulation box along the x and y directions respectively, with $L_x > L_y >> b_0$.

on the separation vector $\vec{\delta}$, which is the relative displacement between opposite crack faces at a point initially joined on the interface. The separation and traction vectors can be resolved into their normal components, $(\delta_n;T_n)$, the normal opening or mode I contribution, and into their tangential components resolved in the direction normal to the crack front, $(\delta_t;\ T_t)$, the shearing or mode II contribution. Our cohesive zone has a linear/softening traction separation law (see Faou et al., 2015 for a complete description). One important feature of the cohesive model we are using is that the interface toughness, $G_c(\psi)$, is following the phenomenological relation proposed by Hutchinson and Suo (1991):

$$G_c(\psi) = G_{Ic}\left[1 + tan^2(\eta\psi)\right]. \tag{2}$$

In this expression, G_{Ic} is the mode I separation energy or toughness and ψ is the mode mixity parameter measuring the mode II to mode I loading ratio at the interface (Hutchinson and Suo, 1991). Finally, η is the parameter controlling the mode mixity's dependence on interface toughness. A value of η close to zero implies a weak dependence on the mode mixity, while a value close to unity provides a strong dependence. In our case, we take $\eta = 0.9$, as for example in Hutchinson and Suo (1991) and Boijoux et al. (2017).

For the loading, a bi-axial compressive stress is first induced in the film by a thermal loading, such that $\sigma_{xx} = \sigma_{yy} = \sigma_0$ and $\sigma_{xy} = 0$, with $\sigma_0 = -570$ MPa. Note that this thermal loading is meant to mimic the stress built-up during the deposition process. The substrate is then compressed along the y direction to induce the nucleation, growth and propagation of two SSBs along the x direction, which is similar to the external loading applied experimentally. The resulting applied stress component in the film along the y axis is noted σ_{yy} in the following.

Finally, different elastic mismatches between the film and its substrate have been investigated and characterized by the Dundur's parameter α, *i.e.* by the film/substrate elastic moduli mismatch. It is assumed that the influence of the second Dundur's parameter β is negligible. For all the calculations, the value of β has been chosen equal to $\alpha/4$, as used in Hutchinson and Suo (1991) and Boijoux et al. (2017). The calculation is carried out using the Green-Lagrange strain tensor to take into account large displacements and properly capture the post-critical shapes of the buckles. The problem was solved using the finite element method (FEM) with the Abaqus software (Abaqus, 2013). The cohesive element (COH) from the Abaqus library was used to model the cohesive zone. The explicit solver has been used to carry out quasi-static simulations.

3.2. Mapping of SSB interactions

The evolution of two SSBs propagating in opposite directions along the x axis is presented in Fig. 4 for various increasing amplitudes of σ_{yy}. The FEM simulations have been carried out for a high elastic contrast, $\alpha = 0.94$, that mimics the experimental case of a Ni film on a polycarbonate substrate. The color contrast corresponds to the out-of-plane displacements along the z axis. The initial separation distance between the two SSBs is fixed to $d = 10\,\mu$m. The two buckles were initiated at two squared areas, with edge length $2b_0 = 5\,\mu$m (see the black dashed squares in Fig. 4a) where the film was debonded from its substrate. As expected (Coupeau et al., 1999; Parry et al., 2006), the increasing amplitude of the stress component along the y direction, σ_{yy}, leads to the propagation of two SSBs along the x axis, in opposite directions (Fig. 4a). The width $2b$ is controlled by the adhesion properties at the lateral crack fronts (Hutchinson and Suo, 1991; Boijoux et al., 2017). It is slightly smaller than 10 µm, *i.e.* quite close to d in this case. As long as the two SSBs are approximately located on each side of a vertical line, a straight propagation of the two SSBs is observed. Once the two propagation fronts cross each other, a significant deviation from the initial straight paths is noticed (Fig. 4b). The two SSBs then seem to be attracted towards each other, in good agreement with the AFM experimental results. It is worth noting that, without any interaction, the SSBs

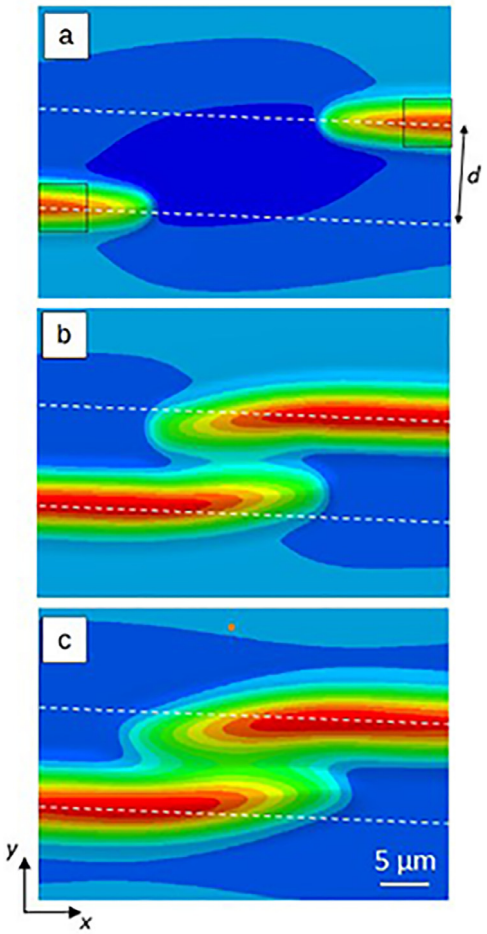

Fig. 4. Equilibrium shapes resulting from two straight-sided buckles propagating in opposite directions for various increasing σ_{yy} stress. Out-of-plane displacements from FEM simulations for $d = 10\,\mu m$, $2b \approx 10\,\mu m$, $h = 200\,nm$ and $\alpha = 0.94$.

would cross the whole simulation box without stopping, which supports the idea of an anchoring phenomenon following the interaction of the two buckles. Finally, once the interaction regime is reached, the propagation has been observed to be more and more difficult, *i.e.* a strong increase of the amplitude of σ_{yy} results in only a slight additional propagation distance along the x direction (Fig. 4c) for each blister.

The different features obtained for various $\bar{d} = d/2b$ values are presented in Fig. 5 for $\alpha = 0.94$. It is observed that the two SSBs do not significantly interact for high $\bar{d}$, leading to a propagation path remaining straight ($\bar{d}$=4.4 in Fig. 5a). For intermediate distances ($\bar{d}$=1.4 in Fig. 5b), the straight path is slightly modified after the crossing of the fronts, but the SSBs continue to propagate. Finally, for $\bar{d}$ close to 1, an arrest of the fronts occurs as previously described, that may be followed by a coalescence of the SSBs (Fig. 5c).

A mapping of occurrence of these three behaviors has been extracted from FEM simulations, as a function of Dundur's parameter α and separation distance $\bar{d}$ (Fig. 6). Since $2b$ may evolve with α (Boijoux et al., 2017), the distance d was here normalized over the particular width $2b^*$ corresponding to the SSB equilibrium width in the case of a hard substrate. The FEM simulations were performed for a given stress amplitude $\sigma_{yy} = 2.3\,GPa$. The three domains are denoted (C), (I) and (N.I.) for the coalescence, interaction and no-interaction areas, respectively. The boundary between (C) and (I) (resp. (I) and (N.I.)) is labeled $\bar{d}_{C/I}$ (resp. $\bar{d}_{I/NI}$). For a given α value, $\bar{d}_{C/I}$ is always smaller than $\bar{d}_{I/NI}$. For $\alpha = -1$ (hard substrate case), $\bar{d}_{C/I}$ is close to 1. A coalescence process was obviously expected for $d < 2b^*$. The interaction domain is shown to be limited to $\bar{d}_{I/NI}$=1.2. It means that, for a hard substrate, the two SSBs do no longer interact above an edge-to-edge critical distance of approximately 20% of their widths. It is shown in Fig. 6 that $\bar{d}_{C/I}$ and $\bar{d}_{I/NI}$ do not significantly evolve with increasing α, up to approximately $\alpha = 0.5$. It is recalled here that such a transition at $\alpha = 0.5$ has been also observed in the past, both impacting the critical buckling stress of a rigid film on a soft substrate (Parry et al., 2005) and the mode mixity at the crack front (Boijoux et al., 2017). For $\alpha > 0.5$, an increase of both $\bar{d}_{C/I}$ and $\bar{d}_{I/NI}$ is observed. The interaction domain (I) that was restricted to approximately two tenth of $2b^*$ for a hard substrate strongly extends as a consequence up to 5 times the SSB width for $\alpha = 0.94$. It is also demonstrated that, even if $d > 2b^*$, two SSBs may coalesce when the elastic contrast between

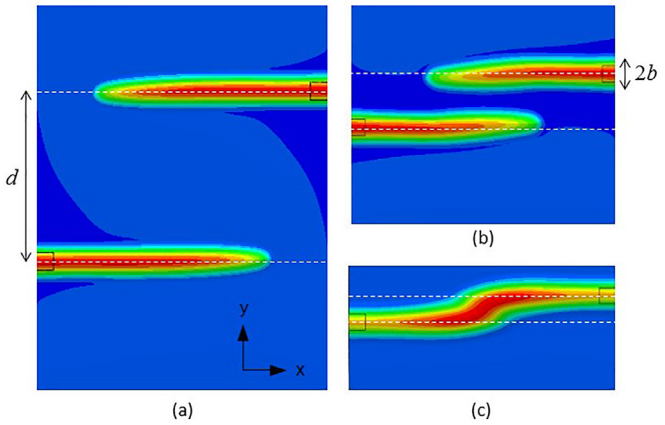

Fig. 5. Equilibrium shapes resulting from two straight-sided buckles propagating in opposite directions for various $\tilde{d} = d/2b$ normalized separation distance (a) $\tilde{d}$= 4.4 (b) $\tilde{d}$= 1.4 (c) $\tilde{d}\approx$ 1. Out-of-plane FEM simulations for $2b \approx 10\,\mu m$, $h = 200\,nm$ and $\alpha = 0.94$.

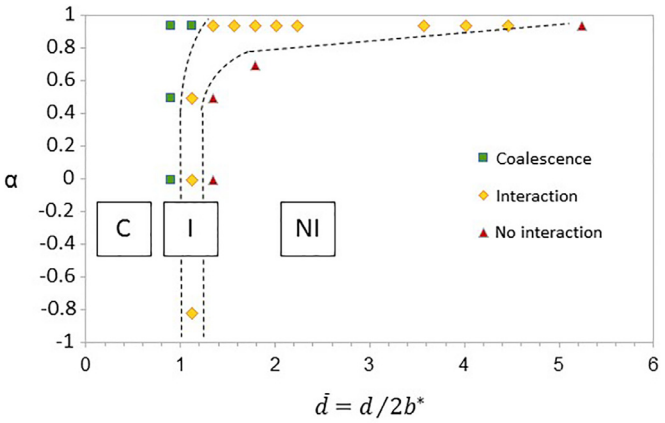

Fig. 6. Interaction mapping of two SSBs as function of α and $\tilde{d}$. d is normalized over the width $2b^*$ of a buckle in the case of a rigid substrate. FEM simulations for $2b^* = 9\,\mu m$, $h = 200\,nm$ and $\sigma_{yy} = 2.3\,GPa$.

the film and the substrate is high enough. For instance, for $\alpha = 0.94$, a coalescence of the two SSBs is still expected if they propagate at an edge-to-edge distance of approximately 25% of their widths.

The influence of stresses σ_{yy} on the SSB interaction has been studied in Fig. 7. The FEM simulations were performed for a given α value equal to 0.94. For low stresses, the propagation of the SSB is not energetically favorable, *i.e.* the elastic energy release rate is lower than the film/substrate interface toughness (Hutchinson and Suo, 1991; Moon et al., 2002; Cordill et al., 2007; Ni and Soh, 2014; Faou et al., 2017). Once the propagation allowed (above a critical stress value equal to 1.85 GPa in our simulation), the mapping for coalescence, interaction or no-interaction is quite similar to the one in Fig. 6. Coalescence obviously occurs for $d < 2b^*$ while the two SSBs do no longer interact for high separation distance d values. It is interesting to note that the boundaries between (C), (I) and (NI) domains do not significantly evolve with the increasing amplitude of the stress component σ_{yy}. It means that the stress is a key factor for nucleation and further propagation of SSBs but does not play any significant role on the interaction process between the SSBs.

3.3. Origin of the SSB interaction

It is now well-known that the stress component σ_{yy} in the case of a film bonded to a rigid substrate can be characterized by a Heaviside function. In the buckled part of the film (for - $b < y < +b$), the stress is relaxed and equal to σ_c, the critical buckling load of the delaminated strip (Hutchinson and Suo, 1991). In the bonded part of the film, for $y > +b$, the stress is constant and equal to the internal stresses of the film. The transition at $y = \pm b$ is thus very sharp for $\alpha = -1$ (hard substrate case). It was also shown by FEM simulations (Parry et al., 2005) that the transition in the stress profile becomes smoother in the case of a compliant substrate; the more compliant the substrate, the smoother the transition. Consequently, the stress in the film asymptotically reaches the internal stress value and the transition is characterized by a characteristic length λ. This length naturally characterizes the distance over which an interaction will occur between two neighboring SSBs. The FEM evolution of the normalized interaction distance, λ/h, is shown in Fig. 8 as a function of α. For practical purpose, λ is

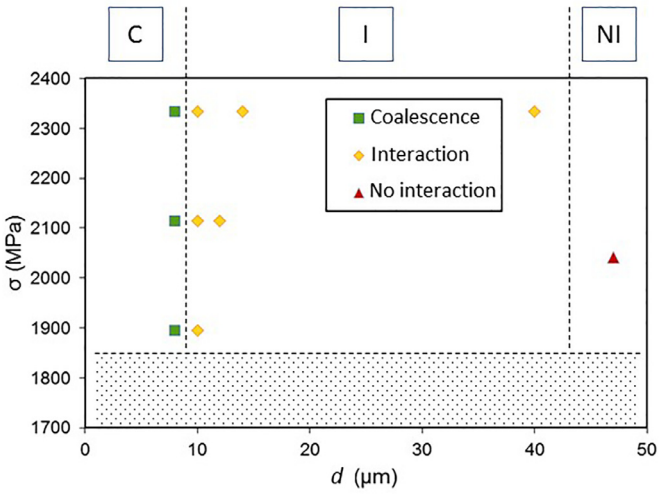

Fig. 7. Interaction mapping of two SSBs as a function of d and σ_{yy}. FEM simulations for $2b^* = 9\,\mu m$, $h = 200\,nm$ and $\alpha = 0.94$.

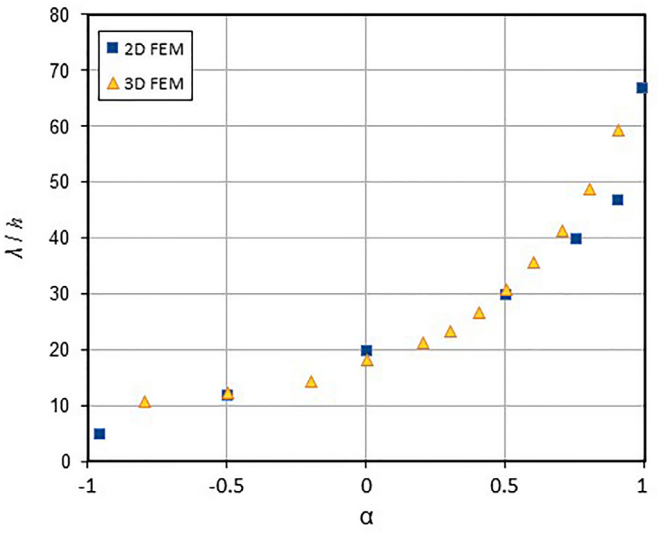

Fig. 8. FEM simulations of the normalized stress field range λ *vs.* Dundur's coefficient α, for a 2D and 3D configuration of the straight-sided buckle.

defined here as the y position from the crack front, for which 99.5% of the internal stresses in the film is recovered. It is shown that λ/h continuously increases with increasing α values. The interaction distance for a very soft substrate is thus increased by more than a factor 5 compared to a hard substrate. It supports the idea that the interaction between two SSBs is enhanced by the film/substrate elastic contrast. Finally, our numerical results are in good agreement with previous FEM simulations based on a 2D modelling (see inserted square points in Fig. 8) (Parry et al., 2005).

The nanometer-scale depression of a SBB has been recently demonstrated to be a relevant signature for extracting the Young's modulus of the film (Boijoux et al., 2018). It is shown in particular a significant increase of the depression depth, for high α values. The depression depth was extracted in this case on each lateral side of the SBB (Boijoux et al., 2018) but no information about the depression at the front itself was given. The depression depth normalized over the maximum deflection, δ_2/δ_1, is presented in Fig. 9 as a function of the x position along the main axis of the SSB, for $\alpha = 0.94$ (FEM simulations). The associated out-of-plane displacement component is also shown in insert. A continuous decrease of δ_2/δ_1 is clearly observed, from around 6% far away from the front to 1.5 % at the apex of the SBB. It indicates that the front of the SSB behaves as in the case of a hard substrate, with an almost vanishing depression. It suggests that, during the crossing of the SSBs, the deviation from their initial straight paths mainly results from subtle effects occurring at the fronts, as experimentally evidenced by AFM.

The fact that the buckles propagate towards each other as they interact may not seem intuitive at first glance. Indeed, following the previous discussion on the stress relaxation in the vicinity of the buckle, it is expected that the strain energy stored in the system is released around the buckles, even more so in the area located in between the two buckles.

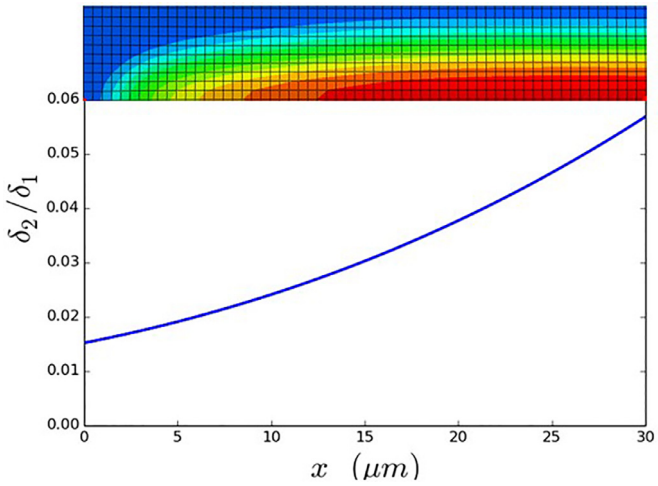

Fig. 9. Normalized depression at the buckle edge δ_2/δ_1 as a function of the x position along the main axis of the straight-sided buckle. FEM simulations for $2b = 10\,\mu m$, $h = 200\,nm$ and $\alpha = 0.94$.

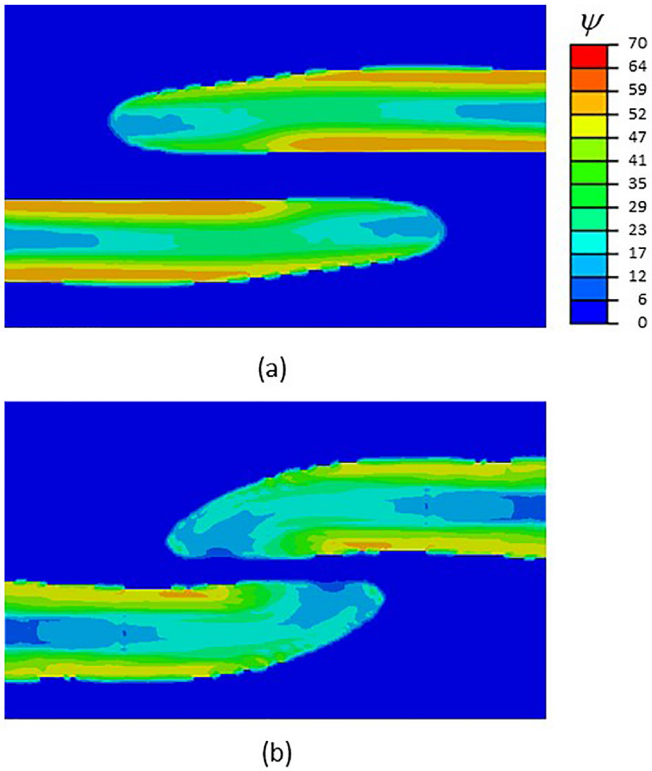

Fig. 10. Mapping of the mode mixity angle ψ (in degrees) at which the interface has been broken during buckle propagation, for two values of the elastic mismatch parameter (a) $\alpha = 0.94$ and (b) $\alpha = 0.99$.

Consequently, the energy release rate G is expected to be lower in between the SSBs, from which a repulsive behavior may have been anticipated instead of the observed attractive behavior. However, it should not be forgotten that the interface toughness is dependent on the mode mixity, so that the real driving force is related to $f(\psi) = G/[1 + tan^2(\eta\psi)]$. Any area of stress distribution ahead of the crack front that would induce a smaller value of ψ would mechanically increase the effective driving force $f(\psi)$. A mapping of the mode mixity parameter ψ at which the interface is broken is reported in Fig. 10, for two values of the parameter α. For both values of α, it is clearly observed that the deviation is associated with a significant decrease of ψ at the crack front and a lower ψ on the internal side (with respect to the other SSB). As a result, the curvature effect is stronger for the highest value of α, with a larger decrease of ψ as well on the internal side (see

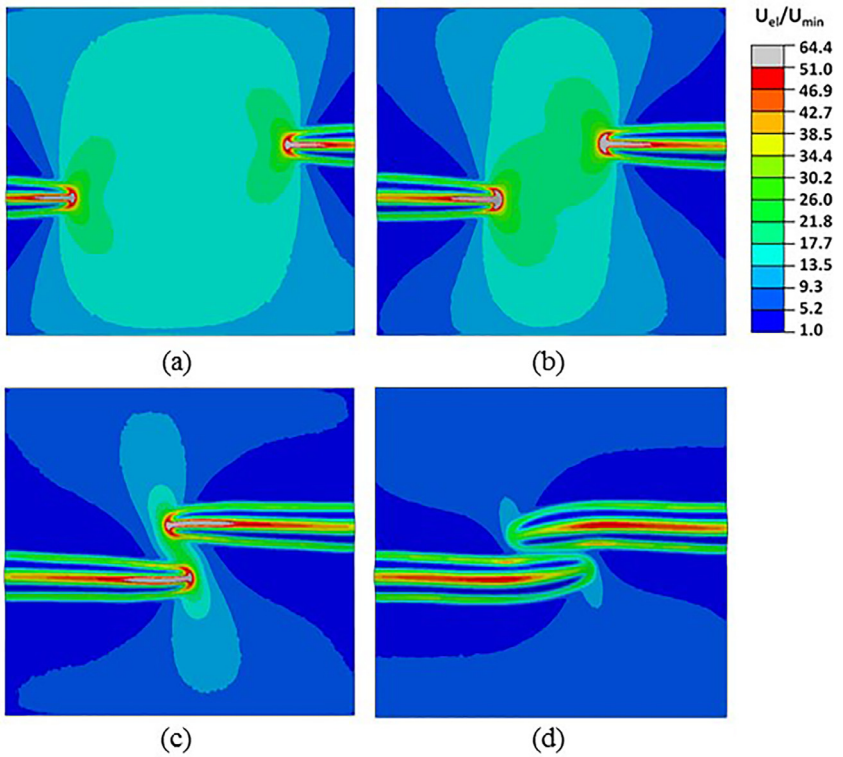

Fig. 11. Strain energy distribution in the film at different stages of buckle propagation, normalized with respect to the minimum value. FEM simulations for $2b = 10\,\mu m$, $h = 200\,nm$ and $\alpha = 0.99$.

Fig. 10b). As far as the lateral extension of the buckles is concerned, it is interesting to notice that the trend illustrated in Boijoux et al. (2017) is verified: a larger value of α is leading to lower values of ψ along the edges and thus to a wider blister ($2b$ is larger for $\alpha = 0.99$ than for $\alpha = 0.94$).

A mapping of the strain energy density at different stages of the SSB propagation is also reported Fig. 11, in the case $\alpha = 0.99$. The energy has been normalized with respect to the lowest value of the energy found in the final configuration. In Fig. 11a, the interaction between the two buckles is still weak, with a rather symmetric energy distribution in the vicinity of each blister. A strong energy density can be found around the head of the buckle, particularly in a butterfly shaped area at its front. Although not illustrated here, it has been observed that the extent of the butterfly shaped energy area is increasing with α, consistent with an increase of the interaction range between SSBs for high values of α. In Fig. 11b, the interaction between the SSBs is well initiated, with an overlap of the energy concentration areas ahead of the buckles. In Fig. 11c, the two buckles have begun to bend their trajectory. This is concomitant with a decrease of the area of high energy at the head of the buckle. Fig. 11d shows the final configuration of the two buckles, on which two remarks can be made. Firstly, the area resulting from the merging of the butterfly regions has been almost completely resorbed. Secondly, the heads of the SSBs, where the highest concentration of energy could be observed in the former propagation steps, have undergone a significant energy relaxation. To conclude, it is also clear from an energetical point of view that the combination of the two SSBs (Fig. 11d) has allowed relaxing a significant amount of energy compared to the configuration of separate wrinkles (Fig. 11a).

4. Conclusion

A model coupling the buckling delamination of a non-linear plate from an elastic substrate using a cohesive zone has been used to study the interaction of two straight buckles propagating side by side in opposite directions. The system, submitted to a loading superimposing an equi-biaxial compressive stress and a uniaxial compression, features mode-dependent interfacial toughness as a key ingredient. The results obtained from FEM simulations correlate well with experimental observations realized *in situ* by AFM on strained coated samples. One remarkable feature is the apparent attraction of the buckles towards each other as soon as their two propagation fronts have been crossing. The interaction range of the buckles is observed to increase with the elastic contrast α. It has been demonstrated here that the propagation front itself is not significantly sinking in the substrate as much as the edges do, suggesting a main front effect. The phenomenon is related to the mode mixity dependence of the interface in a rather subtle way. The symmetry of the loading as seen by a buckle is broken

by the other. In particular, a buckle will find a path with rather small values of the mode mixity ψ when approaching the other one, which means a lower energy to be spent in order to break the interface. In the meantime, approaching its partner allows each buckle to release a large amount of elastic energy over a short distance, in particular the energy originally stored in the strongly strained head region of the buckles. It has also been possible to obtain a phase diagram characterizing the interaction distance between the blisters as a function of the elastic mismatch α. These results will give new insights on the understanding of the buckling phenomenon and more particularly of the elementary interaction mechanisms required for any process of patterning based on compression of elastic films on compliant substrates.

Acknowledgements

This work was funded by the French National Research Agency program "CAPRICE" (ANR-14-CE07-0024-03) and pertains to the french government program "Investissements d'Avenir" (LABEX INTERACTIFS, ANR-11-LABX-0017-01). Y. Ni was supported by the Strategic Priority Research Program of the Chinese Academy of Sciences (Grant No. XDB22040502).

References

Abadias, G., Chason, E., Keckes, J., Sebastiani, M., Thompson, G.B., Barthel, E., Doll, G.L., Murray, C.E., Stoessel, C.H., Martinu, L., 2018. Review article: stress in thin films and coatings: current status, challenges and prospects. J. Vacuum Sci. Technol. A 36, 020801.

Abaqus Manuals Collection, Dassault Systems; Simulia Corp., Providence, RI, USA, 2013.

Abdallah, A.A., Bouten, P.C.P., den Toonder, J.M.J., de With, G., 2008. The effect of moisture on buckle delamination of thin inorganic layers on a polymer substrate. Thin Solid Films 516, 1063–1073.

Audoly, B., Roman, B., Pocheau, A., 2002. Secondary buckling patterns of a thin plate under in-plane compression. Eur. Phys. J. B 27, 7–10.

Boijoux, R., Parry, G., Faou, J.Y., Coupeau, C., 2017. How soft substrates affect the buckling delamination of thin films through crack front sink-in. Appl. Phys. Lett. 110, 141602.

Boijoux, R., Parry, G., Coupeau, C., 2018. Buckle depression as a signature of young's modulus mismatch between a film and its substrate. Thin Solid Films 645, 041405.

Charitidis, C.A., 2010. Nanomechanical and nanotribological properties of carbon-based thin films: a review. Int. J. Refractory Metals Hard Mater. 28, 51–70.

Cordill, M.J., Bahr, D.F., Moody, N.R., Gerberich, W.W., 2007. Adhesion measurements using telephone cord buckles. Mater. Sci. Eng. A 443, 150–155.

Coupeau, C., Girard, J.-C., Grilhé, J., 1998. Plasticity study of deformed materials by *in situ* atomic force microscopy. J. Vacuum Sci. Technol. B 16, 1964–1970.

Coupeau, C., Naud, J.F., Cleymand, F., Goudeau, P., Grilhé, J., 1999. Atomic force microscopy of *in situ* deformed nickel thin films. Thin Solid Films 353, 194–200.

Faou, J.-Y., Parry, G., Grachev, S., Barthel, E., 2015. Telephone cord buckles-a relation between wavelength and adhesion. J. Mech. Phys. Solids 75, 93–103.

Faou, J.-Y., Grachev, S., Barthel, E., Parry, G., 2017. From telephone cords to branched buckles: a phase diagram. Acta Materialia 125, 524–531.

Faulhaber, S., Mercer, C., Moon, M.-W., Hutchinson, J.W., Evans, A.G., 2006. Buckling delamination in compressed multilayers on curved substrates with accompanying ridge cracks. J. Mech. Phys. Solids 54, 1004–1028.

Gioia, G., Ortiz, M., 1998. Determination of thin-film debonding parameters from telephone-cord measurements. Acta Mater. 46, 169–175.

Hutchinson, J., Suo, Z., 1991. Mixed mode cracking in layered materials. In: Advances in Applied Mechanics. Elsevier, pp. 63–191.

Karlsson, B., Valkonen, E., Karlsson, T., Ribbing, C.-G., 1981. Materials for solar-transmitting heat-reflecting coatings. Thin Solid Films 86, 91–98.

Jagla, E.A., 2007. Modeling the buckling and delamination of thin films. Phys. Rev. B 75, 085405.

Moon, M.W., Jensen, H.M., Hutchinson, J.W., Oh, K.H., Evans, A.G., 2002. The characterization of telephone cord buckling of compressed thin films on substrates. J. Mech. Phys. Solids 50, 2355–2377.

Ni, Y., Soh, A.K., 2014. On the growth of buckle-delamination pattern in compressed anisotropic thin films. Acta Materialia 69, 37–46.

Ni, Y., Yu, S., Jiang, H., He, L., 2017. The shape of telephone cord blisters. Nature Comm. 8, 14138.

Pan, K., Ni, Y., He, L., 2013. Effects of interface sliding on the formation of telephone cord buckles. Phys. Rev. E 88, 062405.

Parry, G., Colin, J., Coupeau, C., Foucher, F., Cimetière, A., Grilhé, J., 2005. Effect of substrate compliance on the global unilateral post-buckling of coatings: AFM observations and finite elements calculations. Acta Materialia 53, 441–447.

Parry, G., Cimetière, A., Coupeau, C., Colin, J., Grilhé, J., 2006. Stability diagram of unilateral buckling patterns of strip-delaminated films. Phys. Rev. E 74, 066601.

Ruffini, A., Durinck, J., Colin, J., Coupeau, C., Grilhé, J., 2012. Effect of sliding on interface delamination during thin film buckling. Scripta Materialia 67, 157–160.

Toth, F., Rammerstorfer, F.G., Cordill, M.J., Fischer, F.D., 2013. Detailed modelling of delamination buckling of thin films under global tension. Acta Materialia 61, 2425–2433.

Tvergaard, V., Hutchinson, J.W., 1992. The relation between crack growth and fracture process parameters in elastic-plastic solids. J. Mech. Phys. Solids 40, 1377–1397.

Xu, X.P., Needleman, A., 1993. Void nucleation by inclusion debonding in a crystal matrix. Model. Simul. Mater. Sci. Eng. 1, 111–132.

Yu, H.H., Hutchinson, J.W., 2002. Influence of substrate compliance on buckling delamination of thin films. Int. J. Fract. 113, 39–55.

Yu, S., Chen, M., Chen, J., Zhou, H., Zhang, Y., Si, P., 2013. Spatial and kinetic evolutions of telephone cord buckles. Surface Coat. Technol. 228, 258–265.

Yu, S., Xiao, X., Chen, M., Zhou, H., Chen, J., Si, P., Jiao, Z., 2014. Morphological selections and dynamical evolutions of bucklingpatterns in SiAlNx films:From straight-sided to telephone cordor bubble structures. Acta Materialia 64, 41–53.